

Nature of the quantum phase transitions in the two-dimensional hardcore boson model

F. Hébert, G. G. Batrouni

Institut Non-Linéaire de Nice, Université de Nice–Sophia Antipolis, 1361 route des Lucioles, 06560 Valbonne, France

R. T. Scalettar

Physics Department, University of California, Davis CA 95616, USA

G. Schmid, M. Troyer

Theoretische Physik, Eidgenössische Technische Hochschule Zürich, CH-8093 Zürich, Switzerland

A. Dorneich

Institut für Theoretische Physik, Universität Würzburg, 97074 Würzburg, Germany

We use two Quantum Monte Carlo algorithms to map out the phase diagram of the two-dimensional hardcore boson Hubbard model with near (V_1) and next near (V_2) neighbor repulsion. At half filling we find three phases: Superfluid (SF), checkerboard solid and striped solid depending on the relative values of V_1 , V_2 and the kinetic energy. Doping away from half filling, the checkerboard solid undergoes phase separation: The superfluid and solid phases co-exist but not as a single thermodynamic phase. As a function of doping, the transition from the checkerboard solid is therefore first order. In contrast, doping the striped solid away from half filling instead produces a striped supersolid phase: Co-existence of density order with superfluidity as a single phase. One surprising result is that the entire line of transitions between the SF and checkerboard solid phases at half filling appears to exhibit dynamical $O(3)$ symmetry restoration. The transitions appear to be in the same universality class as the special Heisenberg point even though this symmetry is explicitly broken by the V_2 interaction.

PACS numbers: 75.10Nr, 05.30 Jp, 67.40.Yv, 74.60.Ge

I. INTRODUCTION

The boson Hubbard Hamiltonian¹ has been studied as a model of the superconductor–insulator transition in materials with preformed Cooper pairs,^{2–7} of Helium in disordered and restricted geometries,^{8–10} of spin–flop transitions in quantum spin systems in external magnetic fields,¹¹ and of supersolid behavior.^{12,13} As with the fermion Hubbard Hamiltonian, the boson model explores the role of correlations in inducing ordered phases of many quantum mechanical particles, and the nature of the quantum phase transitions between these phases. However, unlike the fermion case where it is very difficult to reach low temperatures away from points of special particle–hole symmetry, Quantum Monte Carlo (QMC) simulations of the doped boson system have no “sign problem” and hence can successfully be performed. Many fascinating and unexpected features arise, for example re-entrant Mott insulating behavior¹⁴, universal conductivity,^{1–5,15} and supersolidity.^{12,13} Indeed, until algorithms are developed to deal with the sign problem in fermion QMC the boson Hubbard Hamiltonian offers us the best opportunity to explore systematically the details of the competition between phases with diagonal and off-diagonal long range order with QMC simulations.

In this paper we extend some of the previous work which established the basic phase diagram of the model^{1,16–18} in order to characterize the detailed critical properties of the transitions between the phases. We

will use two recently developed algorithms. The first^{19,20} is based on a duality transformation which enables an exact mapping of the boson Hubbard Hamiltonian onto a model of conserved currents, and the second^{22,23} is based on a stochastic series expansion of the imaginary time evolution operator.

The paper is organized as follows: We will first review the definition of the boson Hubbard model and some of its basic qualitative properties. We will then provide a brief review of the two numerical algorithms we employ. Our presentation of the results begins with a discussion of the half-filled system which focusses on a scaling analysis of the transition from a strong coupling solid to a weak coupling superfluid phase. Next, away from half-filling, we discuss the nature of the coexistence of the solid and the superfluid. Finally, we present some concluding remarks and open questions.

II. THE BOSON HUBBARD MODEL

The hardcore boson Hubbard Hamiltonian is,

$$H = -t \sum_{\langle \mathbf{i}, \mathbf{j} \rangle} (a_{\mathbf{i}}^\dagger a_{\mathbf{j}} + a_{\mathbf{j}}^\dagger a_{\mathbf{i}}) + V_1 \sum_{\langle \mathbf{i}, \mathbf{j} \rangle} n_{\mathbf{i}} n_{\mathbf{j}} + V_2 \sum_{\langle \langle \mathbf{i}, \mathbf{k} \rangle \rangle} n_{\mathbf{i}} n_{\mathbf{k}}. \quad (1)$$

$a_{\mathbf{i}}$ ($a_{\mathbf{i}}^\dagger$) are destruction (creation) operators of hard-core bosons on site \mathbf{i} of a 2-d $L \times L$ square lattice, and $n_{\mathbf{i}}$ is the density at site \mathbf{i} . The hopping parameter is chosen to be $t = 1$ to fix the energy scale. V_1 (V_2) is the near (next near) neighbor interaction.

For weak couplings, the ground state of the Hamiltonian is a superfluid. Increasing the near neighbor interaction strength, V_1 , at half filling drives a transition to a checkerboard solid phase where the sites are alternately occupied and empty. This phase is characterized by a vanishing superfluid density, ρ_s , long range density-density correlations, and a gap in the energy spectrum reflected, for example, as a vanishing compressibility, κ , and corresponding plateau in a plot of density ρ versus chemical potential μ . Increasing the next near neighbor interaction strength V_2 at half filling can likewise drive a transition to a striped solid, where horizontal (or vertical) lines of sites are alternately occupied. This phase also has $\rho_s = 0$, $\kappa = 0$ and long range density-density correlations.

At $V_2 = 0$, and after an appropriate sublattice spin rotation, the hard-core boson model is equivalent to the spin- $\frac{1}{2}$ antiferromagnetic XXZ model, with half-filling corresponding to the zero magnetization sector. The hopping t maps onto $J_x/2$ while the interaction strength V_1 maps onto J_z and the chemical potential μ is related to the magnetic field as $h = \mu - zV_1/2$, where z is the number of nearest neighbors of a lattice site. In this language, superfluid order corresponds to magnetic order in the XY plane, while density order corresponds to magnetic order in the Z direction. The boson superfluid-cdw insulator phase transition at $V_1 = 2t$ corresponds to the XY-Ising change in universality class at $J_x = J_z$. At this, the Heisenberg point, the Hamiltonian has an $O(3)$ symmetry and as a consequence the critical temperature is driven to $T_c = 0$. This symmetry is explicitly broken for other values of V_1 or for nonzero V_2 . The boson-Hubbard model with nonzero V_2 also has a spin analog, namely to a Hamiltonian with next-near neighbor exchange.

The behavior of the boson-Hubbard model away from half-filling is considerably more complex. While the compressibility surely becomes nonzero, so that the state is not a Mott insulator, it is possible that, despite doping, the charge correlations remain long ranged. If the doped holes are mobile and interspersed with the density ordered bosons, one has simultaneous superfluid order. On the other hand, the doped holes might phase separate leaving distinct regions of the lattice with superfluid and charge ordering. We will carefully explore these alternate possibilities and describe the nature of the transitions between them.

III. THE MONTE CARLO ALGORITHMS

Until relatively recently, algorithms to simulate interacting quantum bosons on a lattice suffered significant

weaknesses. Most importantly, they had problems with extremely long autocorrelation times, which, as in classical Monte Carlo, were caused by the inability of local changes to move configurations effectively through phase space. A related difficulty was that local moves also resulted in global conservation laws which limited the accessible regions of phase space and hence the measurements that could be performed. In the last several years, “cluster” and “loop” algorithms have very successfully addressed some of these problems.²⁴ Unfortunately, these algorithms do not work equally well in all regions of parameter space, notably away from half filling. In addition, they are not simple to implement when the Hamiltonian is made more complex, e.g. with the inclusion of disorder or longer range interactions.²⁵ In this section we review two approaches which have short autocorrelation times but also are easily implemented for these more general models.

Dual Algorithm: To perform efficient boson simulations we use a newly developed QMC algorithm based on the exact duality transformation of the Bosonic Hubbard model.^{19,20} This approach begins by expressing the partition function as a path integral over coherent states. To implement the duality transformation exactly we followed the method of Ref. 21. The result is that hard-core bosons are represented by conserved “currents” that propagate in the positive imaginary time direction and which can make jumps in any spatial direction. The path integral is transformed into a sum over all deformations of the currents, very much like the world line algorithm. This formulation is similar to that of Refs. 2,3 in that it relies on the duality transformation, but different in that this transformation is exact in our case. Consequently, with our algorithm we simulate the true hard-core Hubbard model, whereas Refs. 2,3 study the very high density (many bosons/site) limit.

The simulation is done in the standard way. A deformation is suggested and it is accepted or rejected in a way satisfying detailed balance. A feature of this algorithm which is not easily implemented in the world line algorithm is that the imaginary time step is not subdivided by a checkerboard break-up, and so a particle can hop several lattice sites at a time. This has the great advantage that it enables us to measure the correlation function of the superfluid order parameter, $\langle a_{\mathbf{i}}^\dagger a_{\mathbf{j}} \rangle$, for large $|\mathbf{i} - \mathbf{j}|$, which is very difficult to measure efficiently in older approaches.

Stochastic Series Expansion: The stochastic series expansion (SSE) algorithm with operator loop update^{22,23} was used for additional calculations on larger systems in the grand canonical ensemble. This algorithm does not suffer from time discretization errors and is one of the most effective algorithm for quantum systems. It has been shown to be as effective as the loop algorithm²⁴ for models where the loop algorithm can be applied. In bosonic models it is better than the loop algorithm, since it does not suffer from the exponential slowing down of

the loop algorithm when the chemical potential is tuned away from half filling.²³

Measurements: The energy E is obtained as the expectation value of the Hamiltonian and is used to determine the chemical potential via the relation $\mu = \partial E / \partial N$, from simulations in the canonical ensemble. Hysteretic behavior in E also provides supporting evidence in characterizing the order of phase transitions.

It is straightforward to measure the density-density correlations and their Fourier transform, the structure factor:

$$c(\mathbf{l}) = \langle n_{\mathbf{j}+\mathbf{l}} n_{\mathbf{j}} \rangle$$

$$S(\mathbf{q}) = \sum_{\mathbf{l}} e^{i\mathbf{q} \cdot \mathbf{l}} c(\mathbf{l}). \quad (2)$$

These quantities characterize the diagonal long range order. Divergence of $S(\pi, \pi)$ in the thermodynamic limit indicates checkerboard order, and in $S(\pi, 0)$ or $S(0, \pi)$ striped order. On finite lattices, the structure factor at the appropriate momentum diverges as the system size in the ordered phase, so that a scaling analysis of simulations on different lattice sizes can demonstrate long range order. From the density itself comes the compressibility which characterizes Mott insulating behavior.

It is also crucial to obtain the winding number, since it will be used to determine the superfluid density $\rho_s \propto \langle W^2 \rangle$, a relationship first emphasized in the context of Quantum Monte Carlo simulations by Ceperley and Pollock.²⁶ While global conservation laws on winding and particle numbers preclude the straightforward evaluation of the superfluid density in the dual algorithm and other traditional world-line approaches, we used methods which circumvent this difficulty.^{16,19} Specifically, we calculate the “pseudo” current-current correlation function at different imaginary times. The “pseudocurrent” is defined as the net number of bosons which jumped in a given direction in one imaginary time step. It can be shown easily that the Fourier transform of this correlation function approaches $\langle W^2 \rangle$ as the (Matsubara) frequency approaches zero.^{16,19}

Meanwhile, the global loop updates of the SSE algorithm allow modifications of the particle number and of the winding numbers. The superfluid density ρ_s can thus be measured directly from the winding number fluctuations in these approaches. Two of us have recently developed a method to measure Green’s functions like $\langle a_i^\dagger a_j \rangle$ in the SSE algorithm. We refer to Ref. 23 for details of this method. Values for the superfluid density obtained via the dual and SSE algorithms, although obtained very differently, are entirely consistent.

IV. PHASE DIAGRAM AND TRANSITIONS HALF FILLING

As we have already described, at half filling, one can easily recognize the existence of at least three phases. For

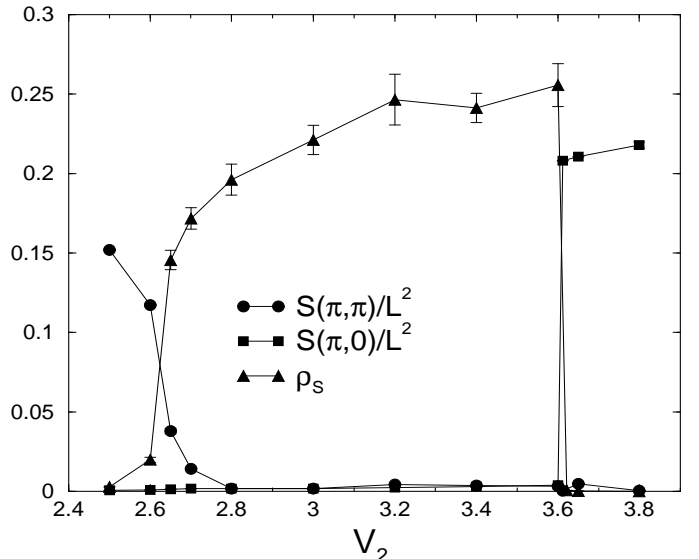


FIG. 1. The structure factor, $S(\pi, \pi)$ (circles), $S(\pi, 0)$ (squares) and the superfluid density, ρ_s (triangles) at half filling for $V_1 = 6$ as functions of V_2 . $L = 12, \beta = 12$

weak V_1 and V_2 it is clear that a superfluid phase exists and, as we will see below, this extends to very strong repulsions when the competing interactions nearly balance. If V_1 dominates, the energy cost of having near neighbors becomes too high and the bosons organize themselves into a checkerboard solid. On the other hand, when V_2 dominates, it is less costly to have near neighbors compared to next near neighbors and the bosons organize themselves in a striped solid. What is not obvious is whether there are other phases, for example supersolids separating the solid phases from the superfluid phase. In previous work^{12,19,20} we demonstrated that at half filling there are no supersolid phases in this model. This is confirmed in the present work where we determine the phase diagram more accurately than before and study in detail the nature of the transitions. The case $V_2 = 0$ and $V_1 = 2$ serves as a good test for our simulations, since it corresponds to the well-understood Heisenberg point of the XXZ model.

The checkerboard and striped solids have structure factors which diverge as L^2 , with momentum ordering vectors (π, π) and $(\pi, 0)$ (or $(0, \pi)$) respectively. Figure 1 shows these two quantities for fixed V_1 as V_2 is varied. We see that as V_2 is increased, $S(\pi, \pi)$ falls to zero, ρ_s takes a finite value while $S(\pi, 0)$ remains zero. This indicates a (π, π) -solid to superfluid phase transition. Increasing V_2 further, ρ_s vanishes abruptly while $S(\pi, 0)$ takes a finite value indicating a superfluid to striped $(\pi, 0)$ -solid.

Putting together the transition points obtained from several such slices, we arrive at the ground state phase diagram in the (V_1, V_2) plane at half filling. This is shown in Fig. 2. Two remarks are in order. It is interesting to note in Fig. 2 that even for very large values of V_1 and V_2 , there is no direct transition between the checkerboard

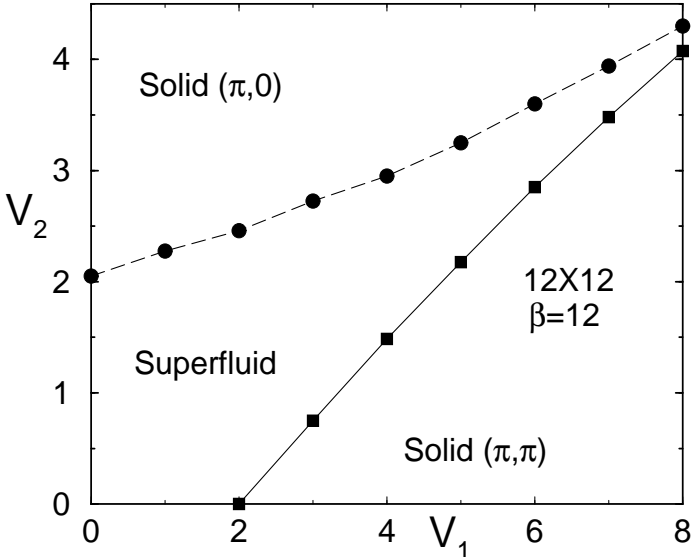


FIG. 2. The ground state phase diagram in the (V_1, V_2) plane. The dashed line indicates first order transitions, the solid line exhibits what appears to be dynamically restored $O(3)$ symmetry except at $(V_1 = 2, V_2 = 0)$ where the symmetry is explicit in the hamiltonian (see text below).

and striped phases: The superfluid phase seems always to intervene. Presumably, the two solid phases eventually meet as both V_1 and V_2 go to infinity. This is in contrast with the mean field result¹² that the two phases meet at $(V_1, V_2) = (4, 2)$. The second remark is that V_2 does not need to be larger than V_1 in order for striped order to win over checkerboard order. For example, $(V_1, V_2) = (6, 4)$ is in the striped phase. This is important because it makes the striped phase more likely to appear physically since one might expect near neighbor repulsion to be stronger than next near neighbor.

Fig. 1 also shows that (π, π) -SF transition appears smooth suggesting a continuous phase transition. This will be examined in detail below. On the other hand, Fig. 1 also shows that the SF- $(\pi, 0)$ transition is very sudden, suggesting a first order transition. To verify the first order nature of the SF- $(\pi, 0)$ transition we look for hysteresis in $S(\pi, 0)$ and $\langle E \rangle$ as V_2 is increased and then decreased, always starting a new simulation from the last configuration of the previous run. The results are shown in Fig. 3. Hysteresis is clearly seen, supporting the evidence for a first order transition. Similar parameter sweeps through the (π, π) -SF transition exhibit no hysteresis.

To determine the order of the transition from checkerboard solid to superfluid we do finite size scaling. Since the Heisenberg point $(V_1 = 2, V_2 = 0)$ is very special (explicit $O(3)$ in the Hamiltonian), we first did the analysis away from it by fixing $V_1 = 3$ and finding the transition as V_2 is changed (see Fig. 1). Since from Fig. 1, the SF to (π, π) -solid transition appears continuous, we will first proceed by assuming a second order transition and car-

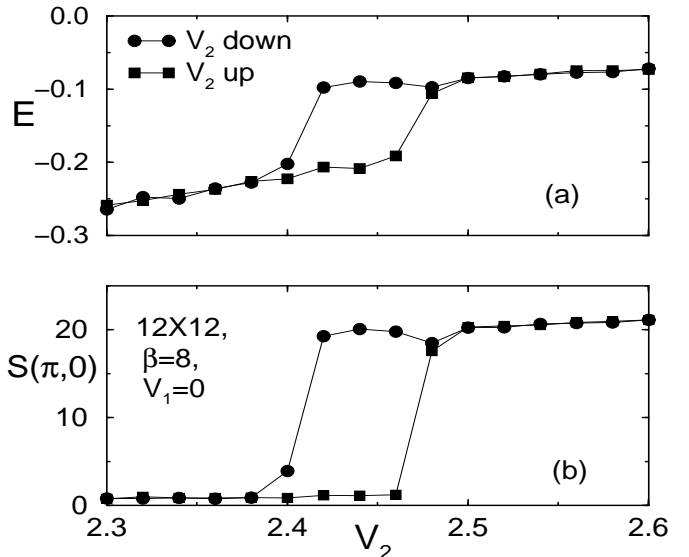


FIG. 3. Hysteresis of (a) the energy E and (b) $S(\pi, 0)$, as V_2 is increased and decreased showing the striped solid to superfluid transition to be first order.

rying out the appropriate finite size scaling. What this analysis will show is that while a quite reasonable data collapse can be achieved, the requisite dynamic critical exponent is anomalously small. This will lead us to perform a more careful analysis which will reveal the true, and more subtle, critical behavior.

In Fig. 4 we show ρ_s versus V_2 for system sizes $L = 6, 8, 10, 12$. In a quantum phase transition, the finite size scaling function not only depends on the appropriately scaled distance to the critical point, but also on the ratio of the lattice dimensions in space and imaginary time. It is standard to assume the following form for the superfluid density¹,

$$\rho_s \propto \frac{1}{L^z} F \left(\frac{V_2 - V_2^c}{L^{-1/\nu}}, \beta/L^z \right). \quad (3)$$

One approach is to simulate several sets of lattice sizes, each set with a different space/imaginary time aspect ratio associated with different guesses for z . Instead, we first use another approach which is to choose the inverse temperature large enough ($\beta = 20$ usually suffices) so that the second argument in F is a constant as L is varied. With this choice, $\rho_s L^z$ must then be independent of L at the critical point. The best intersection was found when $z = 0.25$, giving a critical interaction value $V_2^c = 0.765$ (see Fig. 4). Replotting this figure using the scaled variable $(V_2 - V_2^c)L^{1/\nu}$ we obtain very good data collapse shown in figure Fig. 5. This collapse yields the value of the correlation function exponent $\nu = 0.36$.

Once these critical exponents were found, we redid the simulations but with the two parameter finite size scaling analysis mentioned above in which the temperature is varied with $L, \beta \propto L^z$, in order to keep the second argument in Eq. 3 constant. This reproduced the same

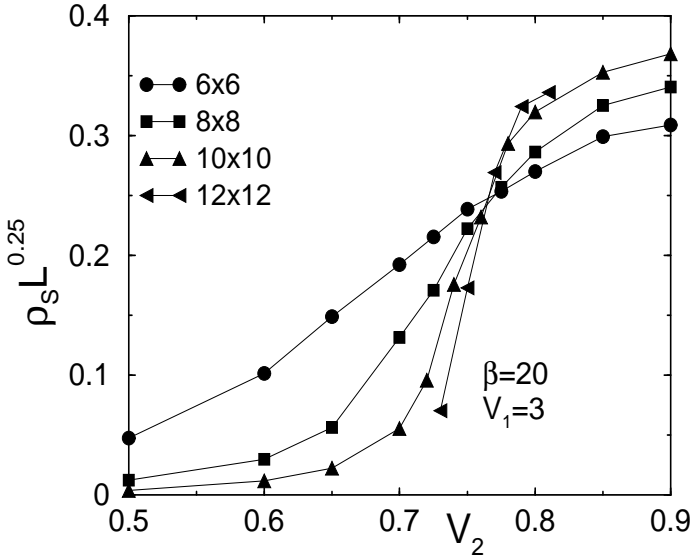


FIG. 4. ρ_s as a function of V_2 for $L = 6, 8, 10, 12$. The intersection gives the critical value $V_2^c = 0.765$.

values found for z and ν .

Scaling analyses and data collapse of this level of quality are rather commonly used to draw conclusions concerning the appropriate critical behavior and universality. However, the value of the dynamical critical exponent, $z = 0.25$, is surprisingly small. All previous debate^{12,27} had been whether $z = 1$ or $z = 2$. This leads us to re-examine the process and, in particular, check the validity of the above finite size scaling analysis, by applying exactly the same assumptions and methodology to the transition at the Heisenberg point, where we know they should not hold. We obtain very similar scaling data, with the same values of z and ν .

The similarity between the behavior of the superfluid density near the Heisenberg point with that at finite V_2 suggests that the entire line of phase transitions separating the SF and (π, π) -solid phases might be in the same class as the Heisenberg point. However, especially given the possibility of generating ‘acceptable’ finite size scaling plots despite the known critical behavior, that we have just demonstrated, this conjecture clearly requires careful testing, which we shall now describe.

The Heisenberg point is very special in that the Hamiltonian has an $O(3)$ symmetry which is explicitly broken everywhere else in the (V_1, V_2) plane. In order for the transition line from the SF to the (π, π) -solid to be in the same universality class, this symmetry must be dynamically restored at the transition. To check this numerically, we first need to determine accurately a transition point away from the special Heisenberg point. To this end, we fixed $V_1 = 3$ and studied, for many values of V_2 and L , the behavior of $S(\pi, \pi)$ and the condensate, $N(\vec{k} = 0) = \tilde{a}^\dagger(\vec{k} = 0)\tilde{a}(\vec{k} = 0)$ where \tilde{a} is the Fourier transform of the destruction operator. The results for $N(\vec{k} = 0)$ are shown in Fig. 6 and indicate

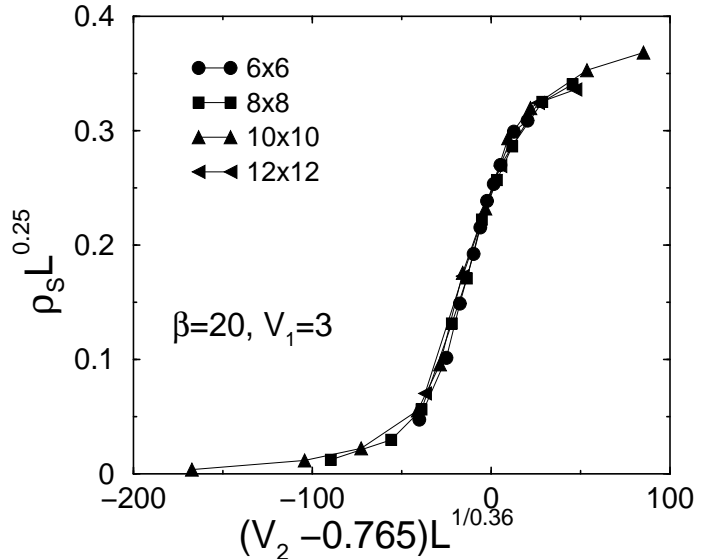


FIG. 5. Same as Fig. 4 but using the scaling variables $\rho_s L^{0.25}$ and $|V_2 - V_2^c|^{1/\nu}$. This yields the values $z = 0.25$ and $\nu = 0.36$.

that the transition happens at $0.760 < V_2 < 0.762$ for $V_1 = 3$. Furthermore, a substantial jump in $N(k)$ is indicated over this narrow window of parameters. This very abrupt transition argues for a discontinuous transition like that at the Heisenberg point.

A sensitive test of this suggestion is that if the $O(3)$ symmetry is indeed restored at the critical V_2 , the transition can only take place at zero temperature. To verify this we did simulations at finite temperature to determine the transition temperatures as a function of V_2 . For $V_2 < 0.761$, the transition is from a normal bosonic liquid to the (π, π) solid, and is expected to be in the 2d Ising universality class. The transition temperatures were determined from crossing points of the 4-th order Binder cumulant ratios $1 - \langle S(\pi, \pi)^2 \rangle / 3 \langle S(\pi, \pi) \rangle^2$ for different system sizes L , and plotted in Figure 7. For $V_2 > 0.761$, the transition is from a normal bosonic liquid to a superfluid, and is expected to be in the 2d XY universality class. The critical temperatures T_{KT} of this phase were determined from the universal jump of the superfluid density ρ_s at the critical temperature. In Fig. 7 we see very clearly that the transition temperature plunges to zero as we approach the critical V_2 . In addition, the way the critical temperature drops to zero is well fitted by $-1/\ln(V_2 - V_{2c})$, just as is the case at the Heisenberg point.

It seems very likely, therefore, that in the ground state, $T = 0$, the transition at half filling from the checkerboard solid to the superfluid proceeds via a dynamical restoration of symmetry and is in the same class as the special Heisenberg point at $V_1 = 2, V_2 = 0$. However, our simulations were done at *finite*, albeit very low, temperatures. Consequently, for the moment, we cannot exclude the possibility that at very low temperatures the transition

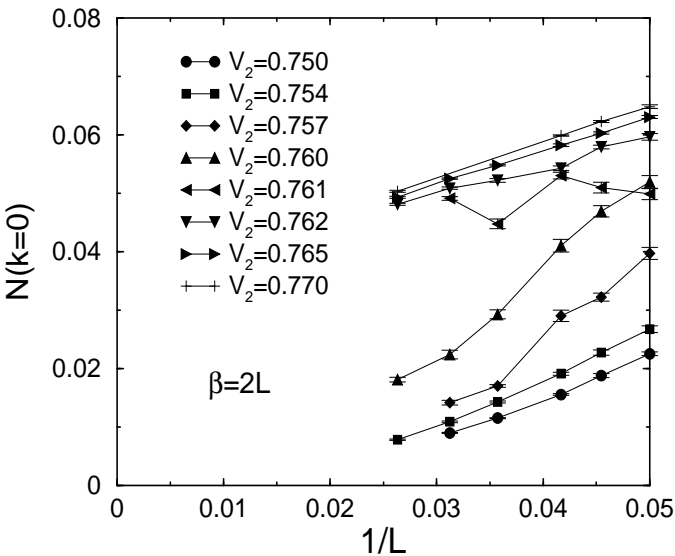


FIG. 6. The number of bosons in the zero momentum mode, the condensate, as a function of $1/L$ for different next near neighbor, V_2 , repulsion values. $\beta = 2L$.

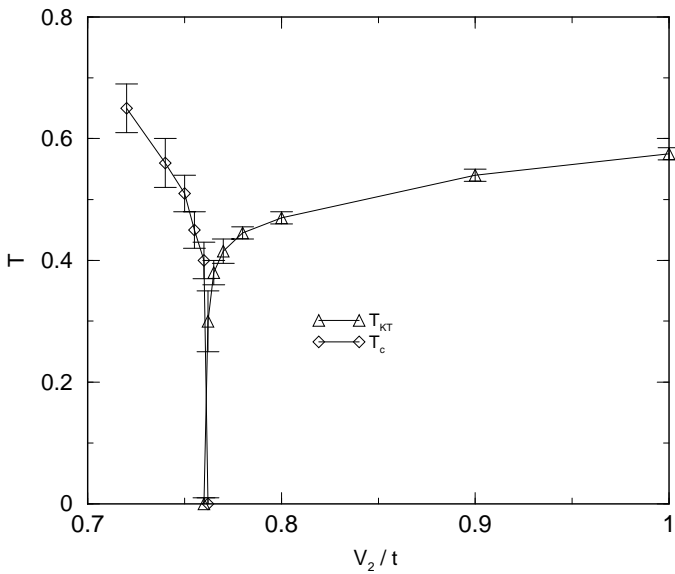


FIG. 7. The transition temperature, T , versus V_2 . At the critical $V_2(\approx 0.761)$ the transition temperature drops to zero. This suggests possible restoration of the $O(3)$ symmetry.

is first order. These issues and the finite temperature phase transition are currently being studied further.³³

It is interesting to compare this with what happens in other systems. In the 2-d extended fermion Hubbard model, there is a similar competition between an anti-ferromagnetic ordered phase and a charge density wave phase. In the case of fermions, the entire zero temperature phase diagram in the (U, V_1) (onsite and near neighbor repulsion) plane at half-filling is believed to be insulating. There is no metallic or superconducting region. This is thought to arise in part because of the peculiar nature of the two-dimensional Fermi surface, which has perfect nesting and a logarithmic divergence of the density of states at half-filling. Both these features act to enhance the tendency for diagonal long range order. However, little has been pinned down precisely as to the nature of the phase transitions in two dimensions. In one dimension, the question has been addressed, and the transition between the two insulating states has been argued to be second order at weak coupling and first order at strong coupling, with an intervening tricritical point.^{28,29} Recent work has called this into question, and suggested that an intervening bond-ordered-wave phase is important.³⁰

In the 1-d soft core boson-Hubbard model, the ground state phase diagram in the U (on-site repulsion) and V_1 (near neighbor repulsion) was also studied extensively¹⁷ at filling $n = 1$. As in the case of 2-d reported here, there is a weak-coupling superfluid phase which is supplanted by ordered, insulating Mott and charge density wave phases at large U and V_1 respectively. A study of hysteresis loops and the free energy barriers indicated that the transition out of the cdw phase to the superfluid is second order at weak coupling, and that the transition from cdw to Mott phase at strong coupling is first order. We see that there are similarities with the 2-d hardcore case reported here, but there also differences, namely here there could be a dynamically restored $O(3)$ symmetry which was explicitly broken in the hamiltonian.

V. DOPED SYSTEM

Now we examine the phase transitions and various phases when the system is doped away from half filling. The hard-core boson-Hubbard Hamiltonian, Eq. 1 has particle-hole symmetry. That is, the transformation $a_i \rightarrow a_i^\dagger$ maps $n_i \rightarrow 1 - n_i$, interchanging occupied and empty sites, but leaves the Hamiltonian unchanged apart from trivial constants. Therefore it is sufficient to do the simulations below half-filling and use this symmetry to calculate physical quantities above.

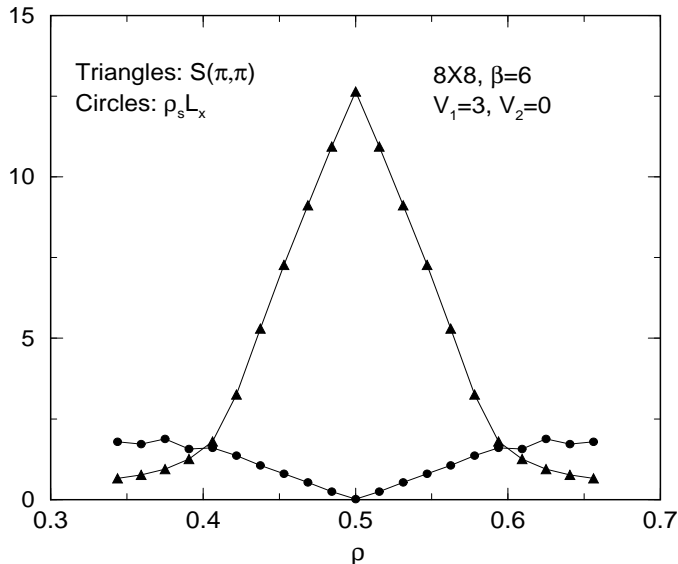


FIG. 8. The structure factor, $S(\pi, \pi)$, and superfluid density, ρ_s , versus the particle density, ρ . For $0.4 < \rho < 0.5$, both ρ_s and $S(\pi, \pi)$ are finite.

A. Evolution of Checkerboard Solid

To explore what happens to the checkerboard solid when the system is doped, we performed a series of simulations at various values of V_1 as the number of bosons in the system is lowered from half filling. We did this mostly with the canonical dual QMC algorithm where the number of bosons is fixed and the chemical potential is calculated from the energy to add a particle to the system,

$$\mu = E(N_{\text{boson}} + 1) - E(N_{\text{boson}}) \quad (4)$$

In Fig. 8 we show a typical result for $V_1 = 3$. At low densities (in this case when $\rho < 0.4$) we see that ρ_s is finite while $S(\pi, \pi)$ is small and decreasing as we move away from $\rho = 0.5$. In addition, finite size studies show that ρ_s is essentially unchanging while $S(\pi, \pi) \rightarrow 0$ for a fixed $\rho < 0.4$ as L grows. Therefore, this corresponds to a superfluid phase. The structure factor reaches its maximum at $\rho = 0.5$ while ρ_s is zero there. This is the checkerboard solid discussed in the previous section.

Between the superfluid phase and the half filling checkerboard solid, *i.e.* for $0.4 < \rho < 0.5$, Fig. 8 shows that both the structure factor and superfluid density are non-vanishing. Furthermore, this is not a finite size effect: For larger systems, ρ_s maintains its value while $S(\pi, \pi)$ diverges with L^2 as it should in the case of long range density wave order. This, therefore, is a candidate for a checkerboard supersolid phase.

To verify this possibility, and check the thermodynamic stability of the supersolid phase we show in Fig. 9 the density, ρ , as a function of the calculated chemical potential, μ . We see that for all the density values where Fig. 8 shows a supersolid, *i.e.* $0.4 < \rho < 0.5$, the

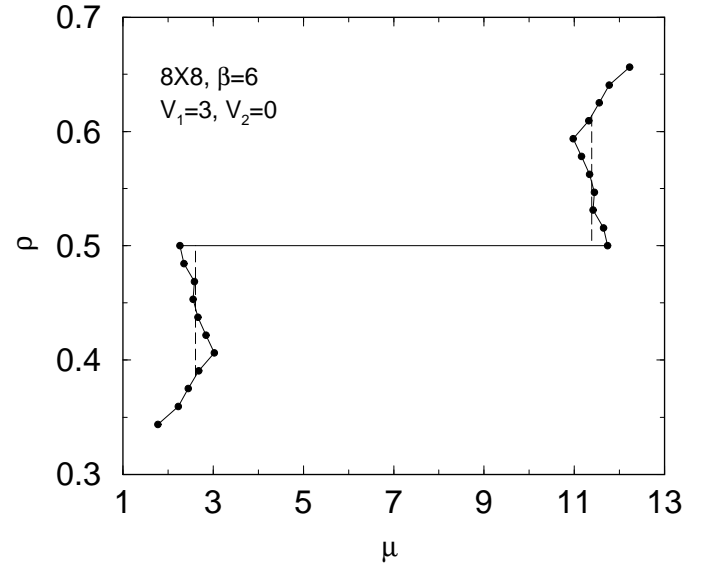


FIG. 9. The particle density, ρ , as a function of the calculated chemical potential, μ . The slope is the compressibility, $\kappa = \partial \rho / \partial \mu$.

curve in Fig. 9 has negative slope and therefore negative compressibility, $\kappa = \partial \rho / \partial \mu$. Consequently, the apparent checkerboard supersolid phase is not stable thermodynamically and undergoes phase separation into a mixture of checkerboard solid and superfluid. This same behavior had previously been established for the magnetization process of the spin-1/2 XXZ model on smaller lattices.¹¹

To establish this phase separation further, we simulated the system in the grand canonical ensemble where μ is the input parameter and ρ is calculated. If the system undergoes phase separation, as shown in Fig. 9, then, for the corresponding value of μ , a histogram of the density should show two peaks, one at $\rho = 0.5$ and the other at $\rho < 0.5$. This is indeed what happens as shown in Fig. 10 for an 8×8 system at $V_1 = 2.86$. The simulation is done for several values of the chemical potential. The phase transition takes place for the μ value with equal peaks. We verified that the peak separation does not change when the system size is increased.

By repeating the simulations that led to Fig. 9 for various values of V_1 , we map out the phase diagram in the $(t/V_1, \mu/V_1)$ plane for $V_2 = 0$. The transitions between the superfluid and the (π, π) -solid phases are first order except at half filling which is the special Heisenberg point. This is shown in Fig. 11. This phase diagram is in agreement with the mean field/spin wave analysis in Ref. 32.

B. Evolution of Striped Solid

Now we investigate the effect of doping on the striped solid phase present at half filling.

The top part of Fig. 12 shows the structure factors,

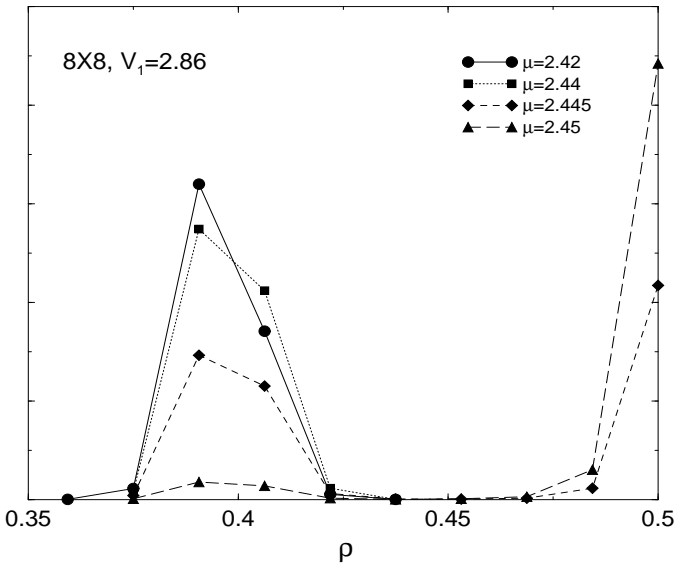


FIG. 10. Histogram of the particle density as the chemical potential, μ is changed. The double peaks show phase separation.

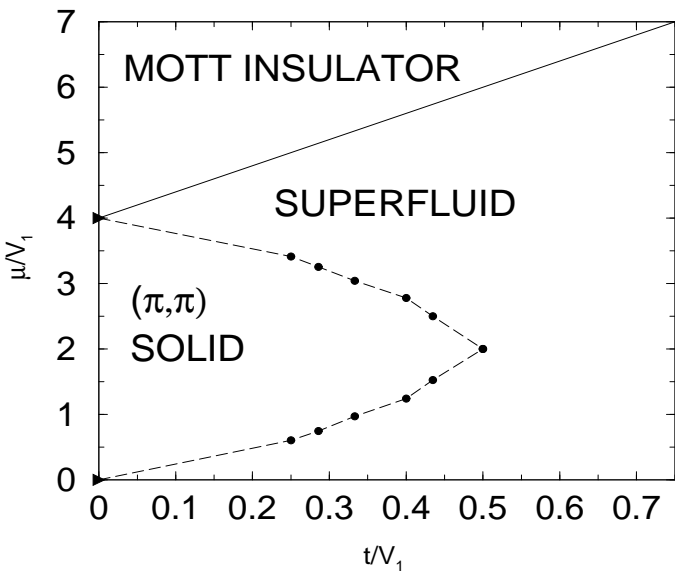


FIG. 11. The phase diagram for $V_2 = 0$. The solid line shows the continuous transition to the Mott phase at full filling, the dashed line shows the discontinuous first order transitions from the superfluid to the checkerboard solid at half filling. The tip of the lobe, $\rho = 0.5$, is the Heisenberg point.

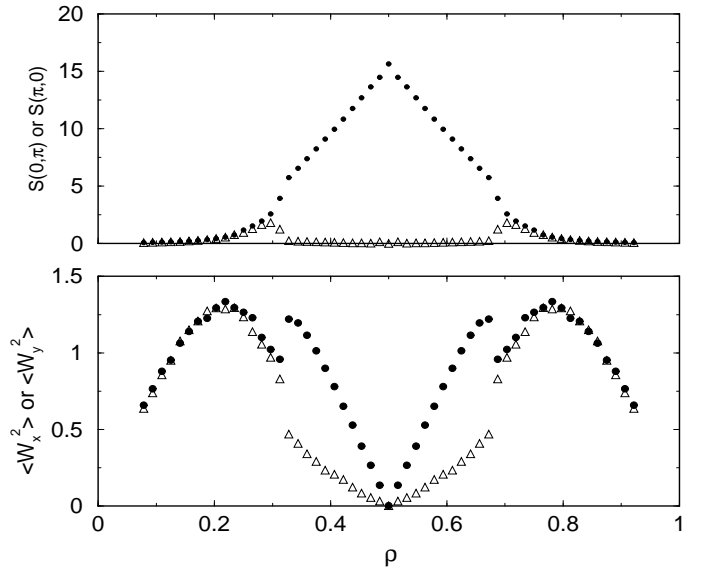


FIG. 12. Top: $S(0, \pi)$ (circles) and $S(\pi, 0)$ (triangles). Bottom: $\langle W_x^2 \rangle$ (circles) and $\langle W_y^2 \rangle$ (triangles). The larger $\langle W^2 \rangle$ (circles) is parallel to the stripes, the lower is transverse. The system is 8×8 , $V_1 = 0$, $V_2 = 5$, $\beta = 6$

$S(\pi, 0)$ and $S(0, \pi)$, for $V_1 = 0, V_2 = 5$. For $\rho < 0.3$ we see that the system is isotropic, $S(\pi, 0) = S(0, \pi)$ and vanishing. For $\rho > 0.3$ the symmetry is broken and one of the two vanishes while the other is large (diverges with the system size). That signals the formation of stripes along the x or y directions. It is remarkable that the stripes start forming at such small densities. The figure also shows that at the same densities where the stripes form, the superfluid density is no longer isotropic, $\rho_s^x \neq \rho_s^y$. The superfluid densities in the x and y directions are defined by: $\rho_s^x = \langle W_x^2 \rangle / 4\beta$ and $\rho_s^y = \langle W_y^2 \rangle / 4\beta$, where W_x (W_y) is the winding number in the x (y) direction. In addition, the figure shows clearly that the superfluid density along the stripes is larger than transverse to the stripes. Nonetheless, the superfluid density in the transverse direction does not vanish. Therefore, once again we apparently have a phase which is both superfluid and solid, thus another candidate for the supersolid phase.

Again we check the thermodynamic stability of the supersolid phase by calculating ρ as a function of μ . This is shown in Fig. 13. We see that the compressibility (slope) never becomes negative indicating that phase separation is absent. In addition, we see that the compressibility increases sharply at $\rho = 0.3$ which is the density at which stripes form (see Fig. 12). This indicates that, contrary to the checkerboard case, the striped supersolid phase is indeed thermodynamically stable and has a higher compressibility than the superfluid phase.

It is worth emphasizing that the striped supersolid is *not* merely a one dimensional superfluid phase along the channels created by the stripes. If this were the case, the superfluid density transverse to the stripes would be vanishingly small, which it is not. In addition, it was

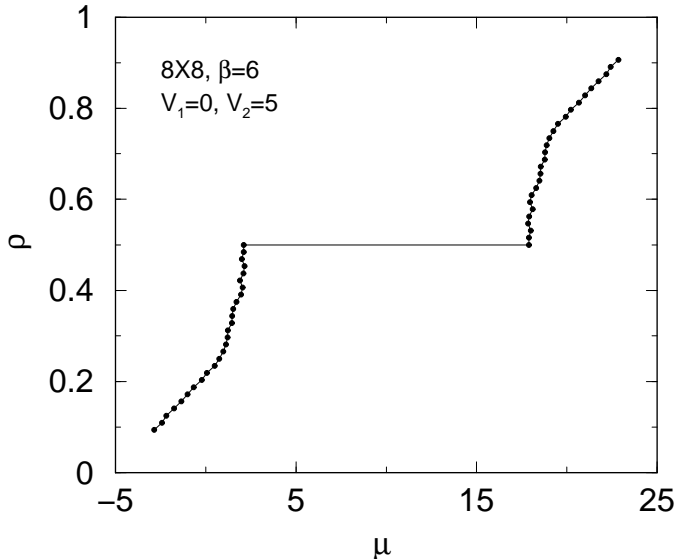


FIG. 13. Particle density, ρ , versus chemical potential, μ . There is a sharp increase in the compressibility as μ is increased when the system goes from the superfluid to the supersolid phase.

shown in Ref. 20 that $\langle a^\dagger(\vec{r})a(\vec{r}') \rangle$ is finite as $|\vec{r}-\vec{r}'| \rightarrow \infty$ transverse to the stripes in the supersolid phase.

By repeating the simulations that led to Figs. 12 and 13, we map out the phase diagram in the $(t/V_2, \mu/V_2)$ plane. This is shown in Fig. 14. The narrow regions sandwiched between SF and $(\pi, 0)$ solid phases are the stable supersolid phases.

As can be seen in Fig. 12, the transition from the SF to the supersolid phase appears to be first order. The transition from the supersolid to the striped solid phase is continuous as is seen from the behavior of the superfluid density as half filling is approached. We see from the lower part of Fig. 12 that both branches of the superfluid density, parallel and transverse to the stripes, go to zero smoothly as half filling is approached. In fact, both branches behave like $|\rho - 1/2|$, indicating a second order transition with a unit exponent.

VI. CONCLUSIONS

The boson–Hubbard model exhibits many fascinating quantum phases and phase transitions. In this paper, we have shown that the detailed critical behavior at those transitions, that is, both the order of the transitions and the critical exponents, can now be determined with recently developed Quantum Monte Carlo algorithms. Our principal conclusion is that, although a first order transition cannot be categorically ruled out at the moment, the superfluid to checkerboard solid transition at half-filling appears to proceed via a dynamical restoration of the explicitly broken $O(3)$ symmetry, and is therefore in the same class as the Heisenberg point. This confirms

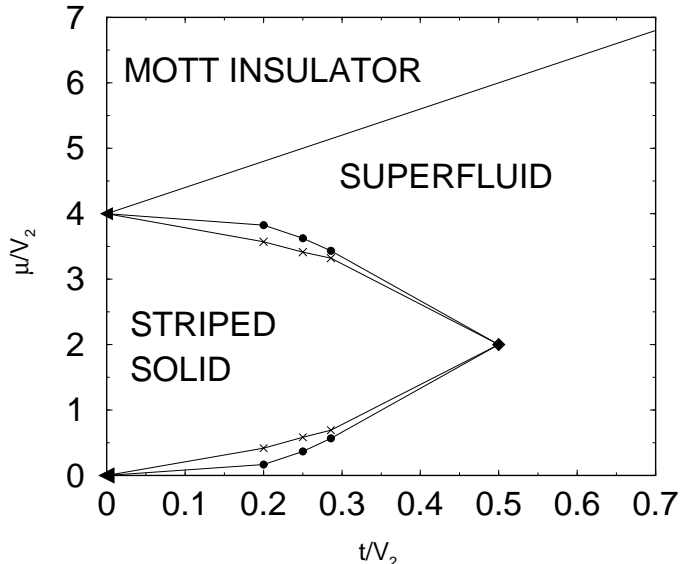


FIG. 14. The phase diagram for $V_1 = 0$. The narrow regions sandwiched between SF and $(\pi, 0)$ solid phases are the stable supersolid phases.

that, for the bosonic Hubbard model at half filling, there is no supersolid phase between the checkerboard solid and superfluid phases¹², unlike what is observed in other models^{27,34}. The details of the finite temperature phase diagram are currently being worked out³³.

In addition, by examining the density histograms from a grand canonical algorithm, we verified again that what was previously thought to be a checkerboard supersolid phase, is in fact a phase separated mixture of superfluid and solid regions.

As for the striped phases, we showed, from the hysteresis of the energy and structure factor, that the superfluid to striped solid transition, *at half filling*, is first order. The transition from the superfluid phase to the striped supersolid phase (away from half filling) also appears to be first order, in disagreement with Refs. 31,32. We also showed, from the behavior of the superfluid density, that the transition from the striped supersolid phase to the striped solid phase is second order with the superfluid density vanishing as $\rho_s \sim |\rho - 1/2|$.

Acknowledgments

We acknowledge useful conversations with E.W. Fire. This work was supported by NSF–DMR–9985978. We also thank ETH-Zurich and HLRS (Stuttgart) for very generous grants of computer time.

- ¹ M.P.A. Fisher, P.B. Weichman, G. Grinstein, and D.S. Fisher, Phys. Rev. **B40**, 546 (1989).
- ² M. Cha, M.P.A. Fisher, S.M. Girvin, M. Wallin, and A.P. Young, Phys. Rev. **B44**, 6883 (1991).
- ³ E.S. Sorensen, M. Wallin, S.M. Girvin, and A.P. Young, Phys. Rev. Lett. **69**, 828 (1992).
- ⁴ G.G. Batrouni, B. Larson, R.T. Scalettar, J. Tobochnik, and J. Wang, Phys. Rev. **B48**, 9628 (1993).
- ⁵ K.J. Runge, Phys. Rev. **B45**, 13136 (1992).
- ⁶ V.F. Elesin, V.A. Kashurnikov, and L.A. Openov, JETP Lett. **60**, 177 (1994).
- ⁷ A.P. Kampf and G.T. Zimanyi, Phys. Rev. **B47**, 279 (1993).
- ⁸ R.T. Scalettar, G.G. Batrouni, and G.T. Zimanyi, Phys. Rev. Lett. **66**, 3144 (1991).
- ⁹ G.T. Zimanyi, P.A. Crowell, R.T. Scalettar, and G.G. Batrouni, Phys. Rev. **B50**, 6515 (1994).
- ¹⁰ K.G. Singh and D.S. Rokhsar, Phys. Rev. **B46**, 3002 (1992).
- ¹¹ M. Kohno and M. Takahashi, Phys. Rev. **B56**, 3212 (1997).
- ¹² G.G. Batrouni, R.T. Scalettar, G.T. Zimanyi and A.P. Kampf, Phys. Rev. Lett. **74** (1995) 2527; R.T. Scalettar, G.G. Batrouni, A.P. Kampf and G.T. Zimanyi, Phys. Rev. **B51** (1995) 8467.
- ¹³ G.G. Batrouni and R.T. Scalettar, Phys. Rev. Lett. **84** 1599 (2000).
- ¹⁴ T.D. Kuhner, S.R. White, and H. Monien, Phys. Rev. **B61**, 12474 (2000).
- ¹⁵ M.C. Cha and S.M. Girvin, Phys. Rev. **B49**, 9794 (1994).
- ¹⁶ G.G. Batrouni, R.T. Scalettar, and G.T. Zimanyi, Phys. Rev. Lett. **65**, 176 (1990).
- ¹⁷ P. Niyaz, R.T. Scalettar, C.Y. Fong, and G.G. Batrouni, Phys. Rev. **B44**, 7143 (1991); G.G. Batrouni and R.T. Scalettar, Phys. Rev. **B46**, 9051 (1992); and P. Niyaz, R.T. Scalettar, C.Y. Fong, and G.G. Batrouni, Phys. Rev. **B50**, 362 (1994).
- ¹⁸ W. Krauth and N. Trivedi, Europhys. Lett. **14**, 627 (1991).
- ¹⁹ G.G. Batrouni and H. Mabilat, Comp. Phys. Comm. **121-122** 468 (1999).
- ²⁰ F. Hébert, G.G. Batrouni, and H. Mabilat, Phys. Rev. **B61** 10725 (2000).
- ²¹ G.G. Batrouni, Nucl. Phys. **B208** 467 (1982); G.G. Batrouni and M. B. Halpern, Phys. Rev. **D30** 1775 (1984).
- ²² A. Sandvik, Phys. Rev. **B59**, R14157 (1999).
- ²³ A. Dorneich and M. Troyer, unpublished.
- ²⁴ H.G. Evertz, G. Lana, and M. Marcu, Phys. Rev. Lett. **70**, 875 (1993); U.-J. Wiese and H.-P. Ying, Phys. Lett. **A168**, 143 (1992); Z. Phys. **B 93** (1994) 147; N. Kawashima, J.E. Gubernatis, and H.G. Evertz, Phys. Rev. **B 50** 136 (1994); N. Kawashima and J.E. Gubernatis, Phys. Rev. Lett. **73**, 1295 (1994), B. B. Beard and U.-J. Wiese, Phys. Rev. Lett. **77**, 5130 (1996).
- ²⁵ Some additional studies of the boson-Hubbard model with disorder include: N. Hatano, Int. J. Mod. Phys. **C7**, 449 (1996); N. Hatano, J. Phys. Soc. Japan **64**, 1529 (1995); J. Kisker and H. Rieger, Phys. Rev. **B55**, 11981 (1997); J. Kisker and H. Rieger, Physica **A246**, 348 (1997);
- ²⁶ E.L. Pollock and D.M. Ceperley, Phys. Rev. **B30**, 2455 (1984) and Phys. Rev. **B36**, 8343 (1987). D.M. Ceperley and E.L. Pollock, Phys. Rev. Lett. **56**, 351 (1986).
- ²⁷ A. van Otterlo, K.-H. Wagenblast, Phys. Rev. Lett. **72**, 3598 (1994), A. van Otterlo *et al.*, Phys. Rev. **B52**, 16176 (1995)
- ²⁸ J.E. Hirsch, Phys. Rev. Lett. **53** 2327 (1984). Phys. Rev. **B31** (1991) 6022.
- ²⁹ J.W. Cannon, R.T. Scalettar, and E. Fradkin, Phys. Rev. **B44** (1991) 5995.
- ³⁰ P. Sengupta, A. Sandvik, and D.K. Campbell, cond-mat/0102141.
- ³¹ E. Frey and L. Balents, Phys. Rev. **B55**, 1050 (1997).
- ³² C. Pich and E. Frey, Phys. Rev. **B57**, 13712 (1998).
- ³³ G. Schmid, M. Troyer and A. Dorneich, unpublished.
- ³⁴ E. Roddick and D. Stroud, Phys. Rev. **B51**, 8672 (1995).